Applied Catalysis B: Environmental 309 (2022) 121222

Contents lists available at ScienceDirect

Applied Catalysis B: Environmental

journal homepage: www.elsevier.com/locate/apcatb

Nano gold coupled black titania composites with enhanced surface plasma properties for efficient photocatalytic alkyne reduction

Qingyuan Bi [a,b,1], Erhong Song [b,1], Jiacheng Chen [c], Muhammad Sohail Riaz [d], Minghui Zhu [c], Jianjun Liu [b,*], Yi-Fan Han [c,*], Fuqiang Huang [b,e,**]

[a] School of Materials and Chemistry, University of Shanghai for Science and Technology, Shanghai 200093, PR China
[b] State Key Laboratory of High Performance Ceramics and Superfine Microstructure, Shanghai Institute of Ceramics, Chinese Academy of Sciences, Shanghai 200050, PR China
[c] State Key Laboratory of Chemical Engineering, East China University of Science and Technology, Shanghai 200237, PR China
[d] School of Materials Science and Engineering, Gwangju Institute of Science and Technology, Gwangju 61005, Republic of Korea
[e] State Key Laboratory of Rare Earth Materials Chemistry and Applications, College of Chemistry and Molecular Engineering, Peking University, Beijing 100871, PR China

ARTICLE INFO

Keywords:
Black titania
Gold nanoparticles
Solar-to-chemical energy conversion
Photocatalytic alkyne reduction
Surface plasma resonance

ABSTRACT

A nanocomposite design is proven for achieving efficient, selective, and robust alkyne semi-hydrogenation through photocatalytic process, which avoids the use of additional heat sources and traditional toxic Pb additives. The gold nanoparticles (Au NPs) coupled crystalline-core@amorphous-shell structured and wide-spectrum-responsive black titania (BT) with enhanced surface plasma properties holds the key to attaining high activity and selectivity. The hot electron injection from conductive BT to the surface of plasmonic Au NPs stimulated by solar light activates the alkynes and directly participates in the selective conversion to overcome the energy barriers. The engineered Au/BT gives a record turnover frequency of 1012 h^{-1} and excellent stability for phenylacetylene semi-hydrogenation under solar light irradiation and shows broad scope toward selective hydrogenation of alkynes containing various substituent groups of $–CH_3$, –OH, and –Cl. The kinetic isotope effects and in situ infrared spectroscopy analysis for structure-activity relationship and reaction mechanism of phenylacetylene reduction were also demonstrated.

1. Introduction

Semi-hydrogenation of alkynes to the desired alkenes ($R_1{\equiv}R_2 + H_2 \rightarrow R_1H = R_2H$) is of great significance in the fine chemical industry for synthesizing polymer materials, resins, drugs, agrochemical, and various active intermediates [1–4]. This reaction as the most fundamental process has attracted ever-increasing attention in both industry and academia. However, the major challenge in selective semi-hydrogenation of alkynes is designing and developing an efficient catalyst for suppressing the over-hydrogenation process ($R_1{\equiv}R_2 + 2H_2 \rightarrow R_1H_2–R_2H_2$); alkenes are more easily hydrogenated to alkanes [2,4–6]. Lindlar catalyst, $Pb(OAc)_2$-modified $Pd/CaCO_3$, has been widely applied to synthesize various alkenes [5,6]. Unfortunately, it shows several serious drawbacks: (i) the indispensable use of highly toxic Pb additives, (ii) the limited hydrogenation substrate scope on terminal alkynes, (iii) Z/E isomerization, and (iv) the migration reactions on unsaturated C=C double bond in olefin products. Moreover, the energy required to facilitate the hydrogenation reaction largely depends on the conventional thermal mode derived from non-renewable fossil fuels [7–10]. From minimizing the reliance on fossil energy and avoiding toxic Pb species, semi-hydrogenation of alkynes through an energy-efficient and environmentally friendly catalytic system is highly desirable.

Photocatalysis involving metal nanocrystals on semiconductors driven by solar energy is a promising approach for selective hydrogenation reactions to reduce power consumption and hazardous materials

* Corresponding authors.
** Corresponding author at: State Key Laboratory of High Performance Ceramics and Superfine Microstructure, Shanghai Institute of Ceramics, Chinese Academy of Sciences, Shanghai 200050, PR China.
E-mail addresses: jliu@mail.sic.ac.cn (J. Liu), yifanhan@ecust.edu.cn (Y.-F. Han), huangfq@mail.sic.ac.cn (F. Huang).
[1] These authors contributed equally to this work.

https://doi.org/10.1016/j.apcatb.2022.121222
Received 12 January 2022; Received in revised form 10 February 2022; Accepted 12 February 2022
Available online 19 February 2022

utilization. However, there are few reports on selective photocatalytic alkynes hydrogenation to alkenes using heterogeneous catalysis [11,12]. Titanium dioxide (TiO_2) is the most widely applied photocatalyst for CO_2 reduction, water splitting, and photoelectrochemistry. However, the full-spectrum solar utilization efficiencies are still very low owing to the large band gap (3.0 and 3.2 eV for rutile and anatase TiO_2, respectively), inadequate visible light response, low carrier concentrations, and weak separation and transportation of photogenerated electron−hole (e^-−h^+) pairs [13–17]. Tremendous progress has been made to narrow the intrinsic band gap of TiO_2 and enhance its response to visible or infrared light [12–22]. We have recently developed several methods, including Al or Mg reduction, H_2-plasma, and non-metal doping for synthesizing various colorful titania [23–29]. Black titania (BT) with unique crystalline-core/amorphous-shell (TiO_2@TiO_{2-x}) structure can significantly enhance the separation and transportation of photoinduced e^-−h^+ pairs and thus the carrier concentrations [23–29]. Meanwhile, significant surface defects like oxygen vacancies (V_o) in BT benefit reactant mole- cules' adsorption [20–22,27–29]. Thus, BT's unique structure and physicochemical properties can endow exceptional solar light absorption and excellent photocatalytic performance for its supported metal nanocatalysts.

Herein, we demonstrate efficient BT-supported gold nanoparticles (Au NPs) for alkynes' solar-light-driven selective photocatalytic hydrogenation to alkenes in mild conditions. It is well known that Au exhibits ultrahigh selectivity in fine chemical synthesis [30–33]. Under light irradiation, Au NPs usually show the typically localized surface plasmon resonance (LSPR) effect, a unique phenomenon in plasmonic metal nanocrystals (e.g., Cu, Ag, Au) [34–37]. The electrons from BT were solar-inspired to the surface of plasmonic Au NPs and formed high-energy electrons, namely hot electrons or energetic electrons [38–41]. The hot electron injection could activate the alkyne by contacting the carbon-carbon triple bond and directly taking part in the selective photocatalytic hydrogenation reaction. The combined effects of semiconductor BT with typical amorphous TiO_{2-x} shell and plasmonic Au NPs can significantly boost the hydrogenation efficiency under solar or even visible light irradiation at room temperature. The defective BT plains serve as a structural motif to support plasmonic Au NPs, provide abundant surface V_o for electron transportation, and bring an effective contact area, increasing the probability of photoinduced charge carriers interacting with the reactants [27–29]. Of significance is that Au/BT exhibits a turnover frequency (TOF) much more significant than those reported in selective photocatalytic hydrogenation of alkynes under mild conditions. No decay in the actual performance during the catalytic process was observed. Furthermore, the versatile Au/BT shows broad scope toward solar-driven semi-hydrogenation of alkynes containing various substituent groups of –CH_3, –OH, –Cl, and so on.

2. Experimental

2.1. Chemicals and materials

TiO_2 (P25, 70% anatase, and 30% rutile), Al_2O_3, and SiO_2 were supplied from Evonik. D_2 (> 97%) and HD (90%) were obtained from Shanghai Research Institute of Chemical Industry CO., LTD. All of the chemicals were supplied by Alfa Aesar and used without further purification.

2.2. Preparation of BT

The preparation of BT was conducted in a two-zone furnace, in which Al and TiO_2 powders were placed separately and then evacuated to a pressure of < 0.5 Pa. After that, Al was heated up to 800 °C, the TiO_2 was heated to 400 °C for 6 h. After the treatments of annealing and pressure release, the BT sample was carefully collected.

2.3. Preparation of Au/BT catalysts

A modified deposition-precipitation (DP) procedure has been employed to prepare the Au/BT catalysts [42]. Briefly, 0.5 g BT powders were dispersed into the desired amounts of an aqueous solution of $HAuCl_4$ (150 mL), and the pH was adjusted to 9.0 by dropwise addition of 0.25 M $NH_3{\cdot}H_2O$. After 6 h stirring at room temperature, the catalyst was washed several times with deionized water until free of chloride ions (using $AgNO_3$ solution for the test) and separated by filtration. The sample was dried at 100 °C in the air for 5 h, followed by a careful reduction with a 5 vol%H_2/Ar stream at 350 °C (ramping rate of 5 °C min^{-1}) for 2 h.

2.4. Preparation of 0.98 wt% Au/TiO_2 and 0.86 wt% Au/ZrO_2 catalysts

Both catalysts were prepared using the similar modified DP method as Au/BT sample. ZrO_2 powders were prepared by a conventional precipitation method following the reported procedure [42]. The TiO_2 and ZrO_2 were used as support materials for Au/TiO_2 and Au/ZrO_2 catalyst, respectively.

2.5. Preparation of 0.85 wt% Au/Al_2O_3 catalyst

The Au/Al_2O_3 catalyst was prepared by DP method. Briefly, the pH of $HAuCl_4$ aqueous solution was brought to 7.0 by adding NaOH (0.5 M), an appropriate amount of the Al_2O_3 support was added to the neutralized solution, and the resulting suspension was stirred at 80 °C for 1 h. The catalyst precursor was separated from the mother liquor, washed with deionized water, dried in air overnight, and calcined in 5 vol% H_2/Ar at 350 °C for 2 h.

2.6. Preparation of 1.0 wt% Au/SiO_2 catalyst

Briefly, an appropriate amount of SiO_2 was introduced into $HAuCl_4$ aqueous solution. After stirring at 75 °C for 1 h, the solution was cooled to 25 °C, and the solution pH was brought to 8.5 by adding 0.25 M $NH_3{\cdot}H_2O$ under stirring. After 6 h stirring at 25 °C the catalyst was washed extensively with deionized water until it was free of chloride ions. The sample was dried at 110 °C in the air for 1 h and reduced in 5 vol% H_2/Ar at 350 °C for 2 h.

2.7. Catalyst characterization

The BET specific surface area of the samples was determined by adsorption- desorption of nitrogen at –196 °C, using Micromeritics ASAP 2460 equipment. The degassing was performed at 300 °C prior to gaining the adsorption isotherm.

The Au loading of the catalysts was attained by inductively coupled plasma atomic emission spectroscopy (ICP-AES) using a Thermo Electron IRIS Intrepid II XSP spectrometer.

X-ray diffraction (XRD) characterization of the samples was carried out on a German Bruker D8 Advance X-ray diffractometer with the Ni-filtered Cu Kα radiation operating at 40 kV and 40 mA.

X-ray photoelectron spectroscopy (XPS) analysis was conducted on the Axis Ultra Photoelectron Spectrometer (Kratos Analytical Ltd.) through a monochromatized Al K_α anode (225 W, 15 mA, 15 kV). The C 1s peak at 284.8 eV was applied as the reference to calibrate the binding energies (BE).

Raman spectra were collected in a Thermal Dispersive Spectrometer with a 10 mW laser operating at the excitation wavelength of 532 nm.

Electron paramagnetic resonance (EPR) spectra were detected using a Bruker EMX-8 spectrometer at 27 °C and 9.44 GHz.

Ultraviolet-visible (UV-Vis) measurement of the solids was recorded at room temperature on a Hitachi U4100 Spectrometer coupled with an integrating sphere and using $BaSO_4$ as reference. The solar absorption was calculated by the following Eq. (1) [28]:

$$A = \frac{\int (1 - T) \cdot S \cdot d\lambda}{\int S \cdot d\lambda} \quad (1)$$

Where A is the solar absorption, T is the reflectance of the sample, S is the solar spectral irradiance (W m^{-2} nm^{-1}), λ is the wavelength (nm), and the $(1-T)\cdot S$ represents the sample absorption of solar spectral irradiance.

Photoluminescence (PL) spectra were collected at 320 nm on a fluorescence spectrophotometer of MODEL Fluoro Max-3 (Horiba, Japan) at room temperature.

A conventional three-electrode system was applied to conduct photocurrent density measurements on an electrochemical workstation (CHI660B). The sample attached to the cleaned glass substrate (ITO, 1×2 cm^2) as a working electrode was obtained through the spin-coating method. The transient photocurrent signals were collected with and without light irradiation generated from a 150 W Xe lamp. A standard Si photodiode was used to calibrate the light intensity.

The photothermic effect was carried out at a thermal infrared imager SC305 (FLIR Ltd., Sweden) with light irradiation from AM 1.5 G Xe lamp solar simulator.

A JEOL 2011 microscope operating at 200 kV equipped with an EDX unit (Si(Li) detector) was applied for the transmission electron microscopy (TEM) investigations.

A JEM 2100F electron microscope operating at 200 kV equipped with an EDX unit (Si(Li) detector) was used for the high-resolution transmission electron microscopy (HRTEM) investigations.

O_2 adsorption and phenylacetylene pulse adsorption measurements were measured using AutoChem HP 2950 apparatus with a quantitative loop from Micromeritics.

CO chemisorption measurements were performed at − 116 °C [42]. A home-made equipment was used for pulse chemisorption. Before chemisorption the following standard pretreatment procedure was applied: the sample (100 mg) was reduced in H_2 flow (40 mL min^{-1}) at 250 °C for 30 min, cooled in H_2 to ambient temperature, purged in He flow and finally hydrated at ambient temperature. The hydration treatment was performed by contacting the sample with a He flow (10 mL min^{-1}) saturated with water. The sample was then cooled in He flow to − 116 °C (attained and maintained by an ethanol-liquid nitrogen cryogenic mixture in a Dewar flask) for CO chemisorption.

2.8. Computational details

The spin-polarized density functional theory (DFT) calculations were performed using the Vienna Ab initio Simulation Package (VASP) [43], with the generalized gradient approximation of Perdew-Burke-Ernzerhof to describe electron exchange and correlation. The plane-wave basis cut-off was 350 eV. The projector-augmented plane wave (PAW) was used to describe the electron-ion interactions [44]. A set of (2 ×4 × 1) k-points were carried out for geometric optimization, and the convergence threshold was set as 10^{-4} eV in energy and 0.05 eV/Å in force, respectively. The models of Au13-TiO_2(101) and Au13-TiO_2(101)-O vacancy were chosen for simulating the charge transfer between Au13 and TiO_2-based systems. For the systems, the adsorption energy E_{ad} between the adsorbate and Au/TiO_2-based system is defined as.

$$E_{ad} = E_t - (E_{Au/TiO2\text{-based system}} + E_{adsorbate}) \quad (2)$$

Where the subscripts t, Au/TiO_2-based system, and adsorbate denote the total energies and the energies of the corresponding substances.

2.9. Photocatalytic activity test

The experiments were carried out in a high-pressure stainless autoclave reactor (50 mL) with a reflux condenser and a quartz window on the top. The solar light irradiation was from a 300 W Xe lamp (Aulight CEL-HX, Beijing), and the power of the light source was calibrated to AM 1.5 by an NREL-calibrated Si cell (Oriel 91150). The visible light was attained using a light reflector of 400–780 nm, and the reflectivity was greater than 95%. Typically, 2 mL solvent of ethanol, a certain amount of substrate (phenylacetylene or other alkynes), and a known amount of catalyst were placed in the reactor. The autoclave reactor was sealed and flushed several times with 0.5 MPa H_2 to remove the air in the reactor, then 2 MPa H_2 was charged. The stirrer (800 rpm) was started when the light was irradiated. The reactor's temperature was kept at room temperature, and the solar light intensity can be changed from 1.0 to 0.6 W cm^{-2}. After a particular time, the autoclave was placed in cool water, and the gas was carefully released. The gaseous mixture was analyzed using a GC Agilent 7820A equipped with a TDX-01 column connected to a TCD. A known amount of internal standard 1,4-dioxane was added into the aqueous product in an autoclave. The reaction mixture was transferred into a centrifuge tube, and the solid catalyst was separated by centrifugation. The product solution was quantitatively analyzed using a GC Agilent 7820A equipped with an HP-5 capillary column connected to a FID. Identification of the products was performed using a GC-MS spectrometer (Shimadzu GCMS-QP2010 SE) and noted that the total carbon balance was > 95%. For the recycling experiment, the centrifuged catalysts from parallel tests were collected and washed with distilled water several times, followed by air-drying at 100 °C for 5 h and 5 vol% H_2/Ar reduction at 350 °C for 2 h. The average TOF values were calculated by the following Eq. (3).

$$TOF(h^{-1}) = \frac{\text{generatedalkene(mol)}}{\text{totalAuamount(mol)} \times \text{time(h)}} \quad (3)$$

The thermocatalytic experiments were carried out with the same procedure as photocatalysis while the external driving force of 60 °C was used.

2.10. Kinetic isotope effect (KIE) experiments

The experiments were performed using the same procedure as above demonstrated. The H_2 or HD, or D_2 were respectively used as a hydrogen source. The conversions of phenylacetylene were kept below 20% for initial TOF calculation.

2.11. In situ diffuse reflectance infrared fourier transform (DRIFT) measurements

In situ DRIFT spectra for photocatalytic semi-hydrogenation of phenylacetylene were performed in the reaction cell (modified Harricks model HV-DR2) that allowed continuous gas flow through the catalyst bed (50 mg). The reaction cell is equipped with a heater, a temperature controller, and a reflux condenser. The spectra were recorded on a Perkin Elmer spectrum 100 FTIR spectrometer (equipped with an MCT detector) with a resolution of 4 cm^{-1}. The DRIFTS cell's dome owns two KBr windows allowing IR transmission and a third window (quartz) allowing transmission of solar light irradiation introduced by a 300 W Xe lamp. Before the test, the sample was pretreated in He flow for 2 h at 200 °C. The temperature was then lowered to ambient temperature, and the background spectrum in the sample's presence was collected. The spectra were then measured by introducing a phenylacetylene-He mixture to the cell at room temperature for 30 min in the dark when the intensities of adsorption peaks reached saturation. Next, the solar light was turned on for 60 min to investigate the conversion, and the spectra of the adsorbed species were recorded.

3. Results and discussion

3.1. Structural characterization and surface defect analysis

The BT sample was prepared from pristine TiO_2 (P25) via a two-zone Al-reduction strategy under vacuum conditions at 400 °C (Fig. S1) [27].

Table 1
Characteristics of TiO_2, BT, and their supported Au catalysts.

Sample	Surface area ($m^2\ g^{-1}$)	Au loading (wt%)	Au particle size (nm)
TiO_2	43.8	–	–
BT	45.6	–	–
Au/TiO_2	44.5	0.98	4.3 ± 0.5
Au/BT	45.9	0.96	4.5 ± 0.5

Series supported gold catalysts of Au/BT and Au/TiO_2 with ca. 1 wt% metal loading and comparable Au particle size (Table 1) were synthesized using modified DP method [42]. The color of BT turned from the white of initial TiO_2 to black after Al reduction, indicative of the primarily enhanced visible light absorption. The clear blue shift of Raman spectroscopy accompanied the slight peak broadening following the Al treatment (Fig. S4) shows the appearance of the disordered surface layer and numerous V_o in the BT sample [45]. This fact was further confirmed by the Ti 2p XPS (Fig. S5) and EPR results (Fig. S6). The weaker PL peak of BT (Fig. S7) demonstrates that crystalline-core/amorphous-shell structured BT samples with numerous surface V_o show a much lower recombination rate of e^-–h^+ pairs under light irradiation [25,27,29]. Moreover, the loaded Au NPs do not change the structure and specific surface area of underlying materials (Table 1). The absence of any Au-containing crystal phases on XRD patterns (Fig. S8) indicates the low Au metal loading and high dispersion of the Au species.

HRTEM images of Au/BT and Au/TiO_2 catalysts depicted in Fig. 1a and b reveal the uniformly dispersed Au NPs with an average particle size of 4.5 nm (Table 1 and Fig. S9) and without aggregation. Note that the Au NP with clear (111) lattice fringes of Au was powerfully anchored on the disordered surface of $TiO_2@TiO_{2-x}$ structure with (101) facet of anatase TiO_2 in core (inset in Fig. 1a). The Au NPs on V_o-rich BT can harvest visible light and create hot electrons for the selective photocatalytic process. The successful load of Au NPs on BT nanosheets was further confirmed by the UV-Vis absorption spectra, as shown in Fig. 1c. Compared to the pristine TiO_2, BT gives strong absorption in the visible region (400−800 nm) due to its unique geometric and band structure. Upon the introduction of the Au NPs, Au/TiO_2 shows a weak and broad LSPR peak at 550 nm [35,37,46–48], while Au/BT catalyst combines the absorption characteristics of both Au/TiO_2 and BT samples, as reflected with the coexistence of a strong LSPR band and an extended absorption tail. The enhanced plasmonic effect on Au/BT can significantly boost photocatalytic efficiency. There is a loss of V_o to some extent for Au/BT catalyst relative to the BT sample during the wet DP process for Au loading, but the core-shell structure and light response properties exhibit no remarkable change. The photothermic conversion efficiency also investigated the solar absorption of these samples under solar light simulator irradiation. As illustrated in Fig. 1d, after light irradiation for 60 s, the temperature of BT and Au/BT increased to 39 and 38 °C, respectively, which are much higher than those of the pristine TiO_2 and

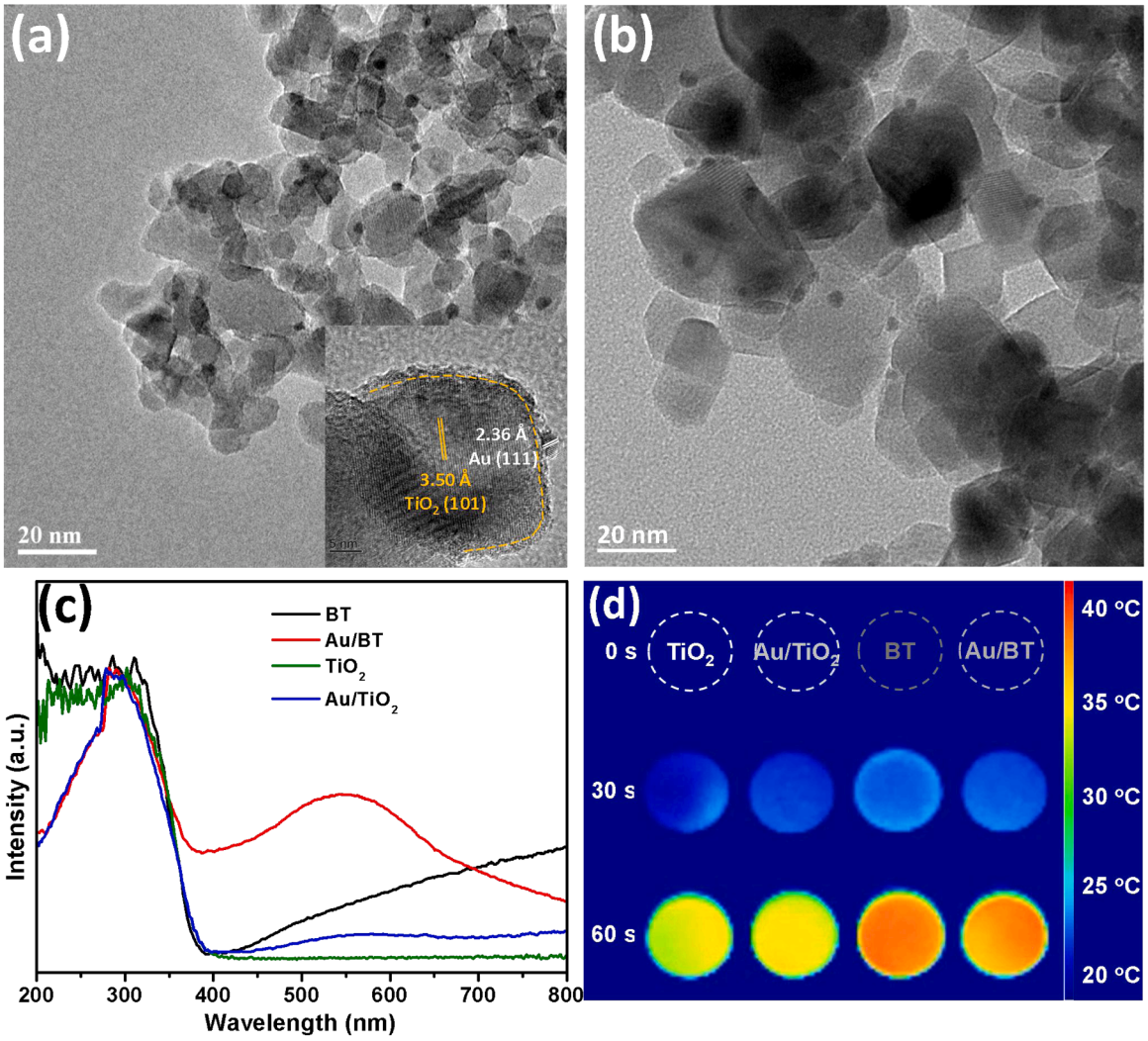

Fig. 1. HRTEM images of (a) Au/BT and (b) Au/TiO_2. Insert in (a) shows the Au NPs supported on the core-shell-structured BT. (c) UV-Vis absorption spectra and (d) thermal image map of cool-pressed disks of BT, TiO_2, and the supported Au samples under solar simulator irradiation.

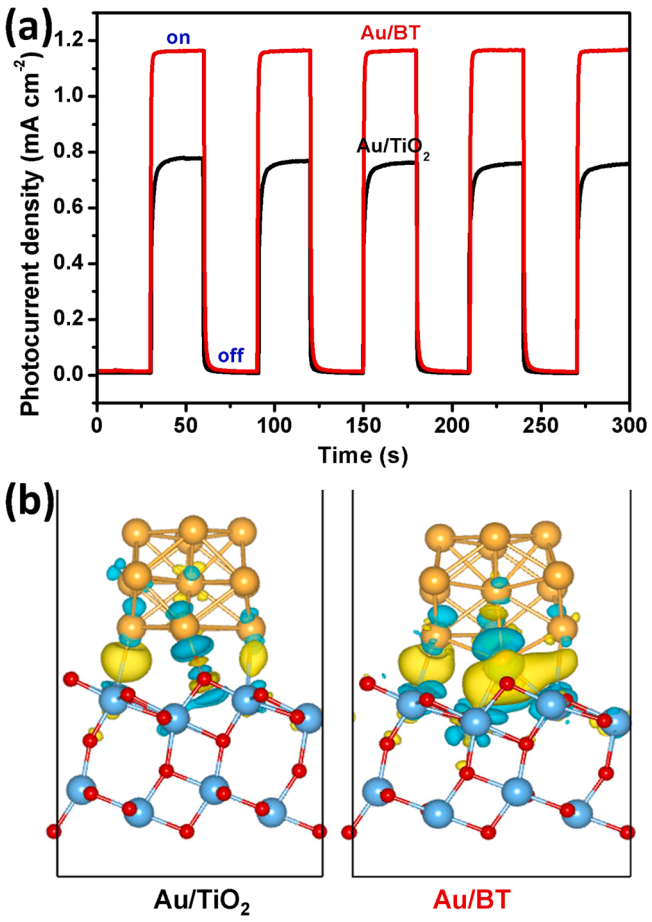

Fig. 2. (a) Transient photocurrent responses and (b) calculated electron density difference contour (yellow zone) for Au/BT and Au/TiO_2 catalysts. Yellow and blue regions represent the accumulation of negative and positive charges, respectively.

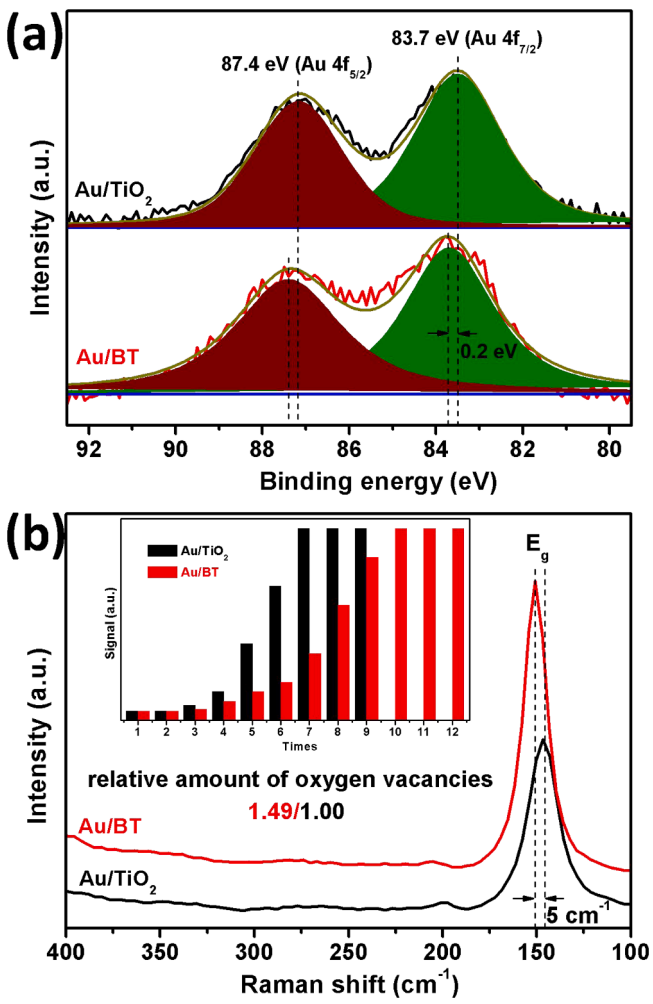

Fig. 3. (a) Au 4f XPS and (b) Raman spectra of Au/BT and Au/TiO_2 catalysts. Inset in (b) is the O_2 pulse adsorption data at room temperature for both Au catalysts.

Au/TiO_2 (both ca. 31 °C).

Furthermore, the defective BT can inject hot electrons to the surface of Au NPs, which makes photocatalysis more efficient. The steady-state photocurrent of Au/BT is 1.16 mA cm^{-2}, which is higher than 0.76 mA cm^{-2} of Au/TiO_2 (Fig. 2a), indicating a more significant concentration of photoinduced carriers or hot electrons in Au/BT during the photocatalytic process [25,27–29]. This fact was further confirmed by the DFT calculation analysis, as the results are depicted in Fig. 2b. Compared to the TiO_2 system, it is found that the defective BT prefers to regulating the electron structure of loaded Au NPs with the larger amount of charge transfer. Thus, the conductive and defective Au/BT catalyst can be widely used as a solar energy harvester for efficient solar to chemical conversions.

Fig. 3a shows the Au 4f XPS results of Au/BT and Au/TiO_2 catalysts. The binding energy of 87.4 and 83.7 eV respective to Au 4f$_{5/2}$ and Au 4f$_{7/2}$ is ascribed to the metallic Au on Au/TiO_2 [42]. A slight upshift of 0.2 eV for Au 4f on Au/BT, indicative of oxide Au species, indicates electron interactions between V_o-rich BT material and Au NPs. It was reported that the surface defects were beneficial for the modulation of the electronic structure of active metal Au and Pd [49,50]. The electron.

transfer also suggests the intimate contact of the Au NPs and the defective BT support. V_o plays an essential role in catalysis, and the slightly positive charged Au NPs are favorable to the catalytic transformation. Raman spectra were recorded to examine the existence of V_o, as depicted in Fig. 3b. The Raman spectroscopy of Au/BT shows a clear blue-shift of 5 cm^{-1} on E_g peak, which indicates Au/BT qualitatively possesses more surface V_o than Au/TiO_2 catalyst [45]. According to the E_g peak area, the relative amount of V_o can be quantitatively calculated, and Au/BT shows approximately 1.49-fold higher than Au/TiO_2 on V_o numbers. The amount of surface V_o was further confirmed by the O_2-titration adsorptions, as the results are shown in the inset in Fig. 3b. The O_2 adsorption amount on Au/BT is much more significant than the value on Au/TiO_2 suggests that the former owns more V_o, thus promotes the adsorption of reactant molecules and overall catalytic efficiency.

3.2. Photocatalytic hydrogenation of alkynes over Au catalysts

The selective photocatalytic hydrogenation of phenylacetylene was chosen as a model reaction to evaluate Au/BT and Au/TiO_2 catalysts' performance. Before the photocatalytic test, the phenylacetylene adsorption experiments were carried out in a dark environment and at room temperature (Fig. S12). The adsorption results show that the physical adsorption process is quickly saturated in a short time, and the phenylacetylene is hard to be desorbed and spontaneously converted downstream without an external driving force. Au/BT sample with larger surface V_o exhibits higher adsorption efficiency for phenylacetylene, which is usually favorable to the subsequent chemical conversion driven by catalysis. Blank experiments without solid catalysts or applying the Au-free BT or TiO_2 display no conversion, further confirming Au species' indispensable role for the desired transformation. Without light irradiation, both catalysts show no activity (Fig. S13). The Au-based samples were found to be highly selective (with the selectivity

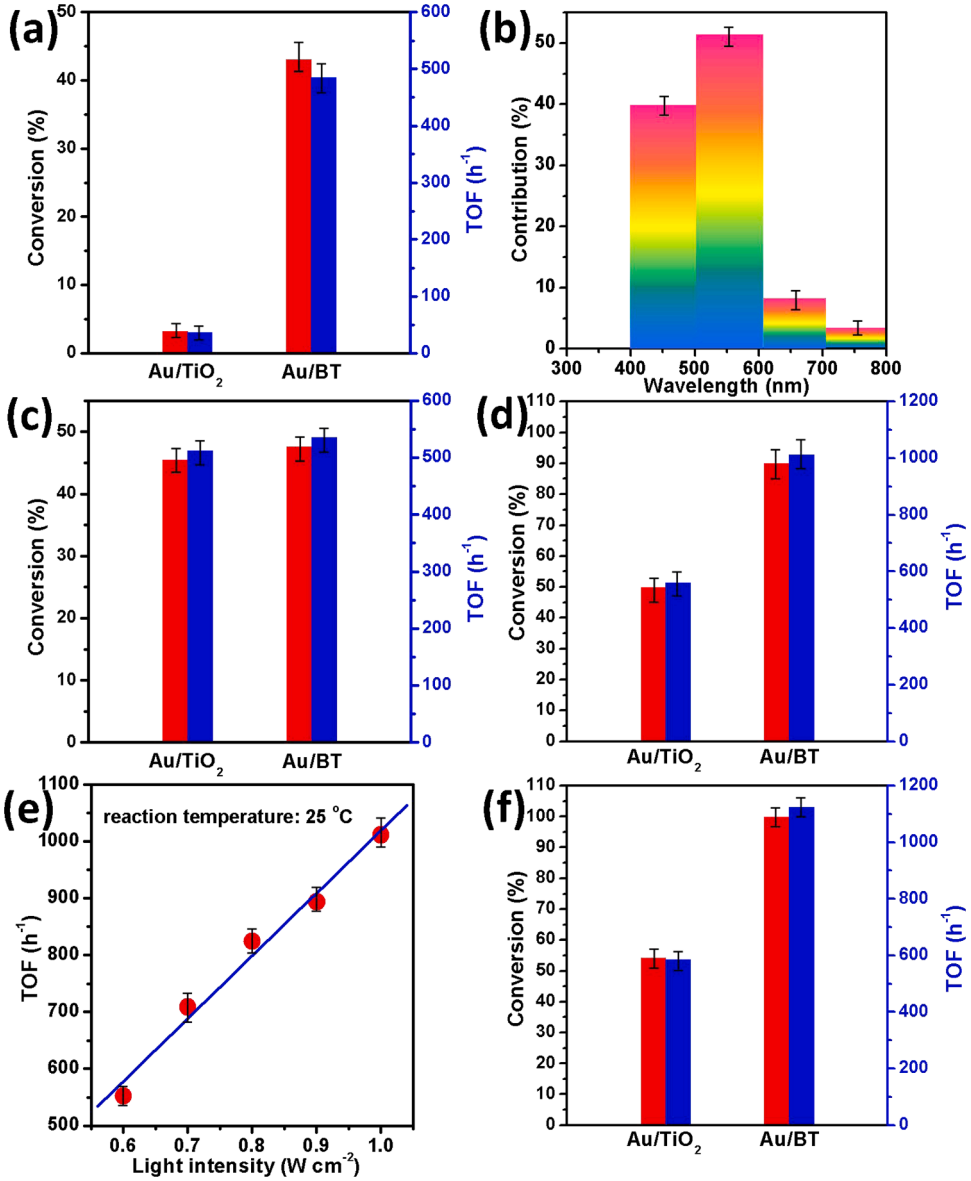

Fig. 4. Selective hydrogenation of phenylacetylene over Au/BT and Au/TiO_2 catalysts. (a) Visible (400 <λ < 800 nm) and (b) visible light wavelength effect for Au/BT at 25 °C; (c) UV light (λ < 400 nm), (d) solar light irradiation at the intensity of 1.0 W cm^{-2}, and (e) solar light intensity effect for Au/BT at 25 °C; (d) thermocatalysis stimulated at 60 °C. Reaction conditions: 40 mg catalyst, 2 mL ethanol, 4.42 mmol phenylacetylene, 2 MPa H_2, 2 h.

of >99%) for styrene synthesis on the mild conditions of 2 MPa H_2 at 25 °C with light irradiation (Fig. 4). The Au/TiO_2 catalyst with a weak response on visible light (400 < λ < 800 nm) shows low phenylacetylene conversion of only 3.2%, while Au/BT gives a higher conversion of 43.1% along with the TOF of 485 h^{-1} (Fig. 4a). The BT can primarily enhance visible light absorption and achieve considerable performance for its supporting Au NPs. For phenylacetylene transformation under visible light irradiation, there is ca. 39% for 400−500 nm, 51% for 500−600 nm, and 10% for 600−800 nm on wavelength effect for Au/BT driving selective phenylacetylene hydrogenation (Fig. 4b). The visible light absorption and the LSPR effect of Au NPs underlying BT in 500−600 nm contribute to the reaction the most. The near-infrared light with 600−800 nm appears to have the most negligible impact on the reaction. The styrene selectivity remains to be > 99% regardless of the range of wavelength.

Furthermore, if the photocatalytic semi-hydrogenation reaction was conducted under UV light irradiation (λ < 400 nm) with the intensity of 1.0 W cm^{-2}, the primarily enhanced conversions with > 99% selectivity of styrene were achieved for both Au catalysts at 25 °C (Fig. 4c). This improved performance is likely due to the intense UV light response and the induced transition of hot electrons in Au NPs under solar light irradiation. Au/BT exhibits significantly enhanced efficiency with ca. 90% conversion and the outstanding TOF of 1012 h^{-1} (Fig. 4d). The observed activity should be directly related to the LSPR effect of Au NPs on versatile BT at 400−800 nm and the synergistic effect between Au species and visible-light-responsive BT support further enhance the conversion. Thus, the hot electrons in Au/BT regulated the reaction pathway to ensure high solar light irradiation performance. The generated hot electrons in the Au NPs surface can activate the phenylacetylene molecules by contacting the unsaturated triple bonds and participating in the selective transformation process. Note that Au/BT sample shows no activity for photocatalytic phenylacetylene semi-hydrogenation in the absence of H_2 source further confirms the photocatalysis feature of the Au catalyst. Remarkably, a near-complete conversion of photocatalytic phenylacetylene semi-hydrogenation can be obtained if enlarged the catalyst dosage or prolongs reaction time.

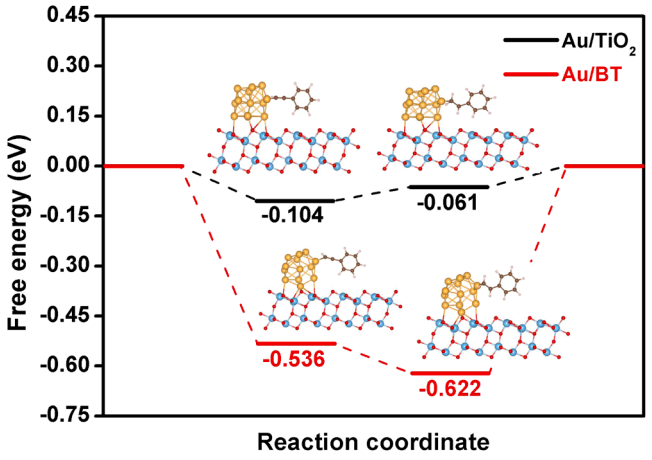

Fig. 5. Free-energy profile for semi-hydrogenation of phenylacetylene to styrene (C_8H_6 to C_8H_8) at Au/TiO_2 and Au/BT catalysts.

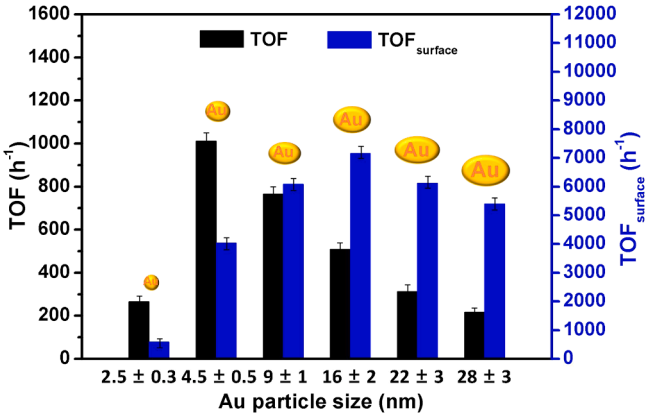

Fig. 6. Effect of Au particle size of Au/BT catalyst on selective photocatalytic hydrogenation of phenylacetylene under solar light irradiation at 25 °C. Reaction conditions: 1.95 μmol Au, 2 mL ethanol, 4.42 mmol phenylacetylene, 2 MPa H_2, 2 h.

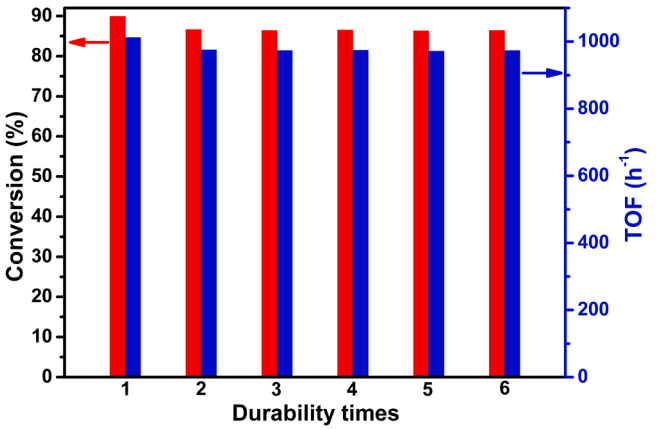

Fig. 7. Recycling Au/BT catalyst for selective photocatalytic hydrogenation of phenylacetylene under solar light irradiation at 25 °C. Reaction conditions for each run: 40 mg catalyst, 2 mL ethanol, 4.42 mmol phenylacetylene, 2 MPa H_2, 2 h.

Emphasized that the exceptional TOF value of Au/BT photocatalysis is more significant than those of previously reported catalysts driven by thermocatalysis (Table S1) [51–63]. Compared to the visible light, UV light can also markedly facilitate the substrate conversion on Au/TiO_2 to 49.8%, accompanying the moderate TOF of 561 h^{-1}. For comparison, the supported catalysts with Au NPs of similar size were examined (Fig. S15). The low performance of Au/ZrO_2 and Au/Al_2O_3 under the solar light irradiation at 25 °C (Table S2) is likely due to the weak response on the full solar spectrum. Au NPs on light-insensitive SiO_2 show no activity under identical conditions, further proves that hot electrons mainly interact with reaction substrates via black titania in Au/BT system. Moreover, the Ag/BT and Cu/BT catalysts with comparable metal particle size were inactive for photocatalytic phenylacetylene semi-hydrogenation under solar light irradiation (Table S2). Thus, the semiconductor's strong light absorption properties are critical for allowing the hot electrons to transfer from the support to the loaded plasmonic metal and the alignment effect between band levels of the defective semiconductor and the Fermi level of the active metal.

For Au/BT catalyst, when the solar light intensity was reduced from 1.0 to 0.9, 0.8, 0.7, and 0.6 W cm^{-2} (measured using the reactor quartz window) under identical experimental conditions, the rate in TOF linearly decreased from 1012 to 894, 825, 709, and 553 h^{-1}, respectively, indicating the semi-hydrogenation process was driven by light irradiation (Fig. 4e). The reduced activity is probably due to the decrease in hot electrons generated at low irradiation intensity. This linear relationship also indicates that the photocatalysis process should be the first order in photon, suggesting that a single photon absorption event dominates phenylacetylene semi-hydrogenation [11]. Besides, we compared the thermocatalytic activity of the selective phenylacetylene hydrogenation using the purely thermal process conducted at 60 °C over both Au catalysts (Fig. 4f). The external heating can achieve a high conversion of 99.8% with the TOF of 1124 h^{-1} for Au/BT. These results illustrate the green, fossil-fuel-independent, and energy-efficient photocatalytic process of selective phenylacetylene hydrogenation over Au/BT with a typical LSPR effect and comparable efficiency with traditional thermocatalysis.

DFT was used to verify the advantage of Au/BT catalyst for hot electron injection boosted styrene synthesis, as the results demonstrated in Fig. 5. The Gibbs free energy profile of photocatalytic semi-hydrogenation of phenylacetylene to styrene at Au/TiO_2 and Au/BT catalysts reveals the corresponding reaction activities. It is found that the free energy of phenylacetylene semi-hydrogenation over Au/BT shows an apparent decrease relative to Au/TiO_2, indicating the defective Au/BT system is beneficial for facilitating the catalytic hydrogenation of phenylacetylene to styrene. Thus, the results reflect the importance of injected hot electrons over V_o-rich Au/BT during phenylacetylene's chemical activation and hydrogenation.

It is well known that the Au particle size significantly affects the catalytic behaviour in many reactions [30–33]. It was reported that the average size of Au NPs in supported gold catalysts could be easily regulated on the nanoscale by changing the initial concentration of gold precursor ($HAuCl_4$) and/or the ageing time during the DP process [42]. Fig. S16 shows the HRTEM images of various Au/BT catalysts with different average Au particle sizes from 2.5 ± 0.3–28 ± 3 nm on the varied preparation conditions. Ultra-small Au NPs of 2.5 ± 0.3 nm displayed low activity due to the weak LSPR effect, as depicted in Fig. 6. With the further increase of Au particle size, the Au/BT catalyst exhibited decreased performance for solar-light- driven selective phenylacetylene hydrogenation markedly from specific activity of 1012 h^{-1} for 4.5 ± 0.5 nm to of 766 h^{-1} for 9 ± 1 nm to of 508 h^{-1} for 16 ± 2 nm. The catalytic ability of 28 ± 3 nm Au NPs coupled BT material was the lowest, displaying the TOF of only 216 h^{-1} under solar light irradiation. However, the Au/BT catalyst with Au particle size of 16 ± 2 nm shows the highest intrinsic activity $TOF_{surface}$ (TOF based on surface gold species). These results reveal that the selective photocatalytic hydrogenation of phenylacetylene over Au/BT composites is a typical particle-size- dependent chemical transformation.

To further confirm whether the Au-catalyzed photoinduced semi-hydrogenation process occurs on the surface of Au/BT, it was removed via filtration from the reaction system after 1 h. Post-processing of the

Table 2
Au/BT-catalyzed selective hydrogenation of alkynes to alkenes under solar light irradiation.[a].

Entry	Alkyne	Target product	Conv. (%)	Sel. (%)	TOF (h^{-1})[b]
1	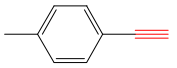	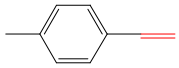	78.2	96.1	771
2	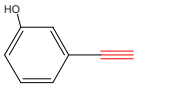	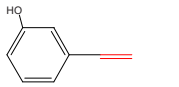	66.4	93.4	636
3	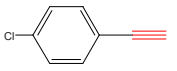	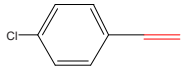	74.9	87.2	670
4	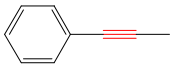	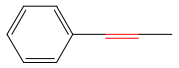	56.5	95.1	551
5	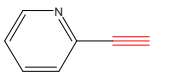	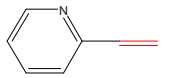	51.4	90.3	476
6	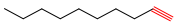		49.8	82.5	420

[a] Reaction conditions: 40 mg catalyst, 2 mL ethanol, 4 mmol alkyne, 2 MPa H_2, solar light irradiation for 2 h.
[b] Average TOF based on alkyne conversion.

resultant filtrate on the identical photocatalytic conditions for another 1 h did not increase the conversion. Furthermore, the ICP-AES analysis of the filtrate shows that the Au or Ti species' content in the solution was below the detection limit, indicating the negligible leaching phenomena occurred during the semi-hydrogenation and the heterogeneous catalysis nature of Au/BT sample. More impressively, the Au/BT catalyst remains relatively stable for selective photocatalytic phenylacetylene hydrogenation to synthesize value-added styrene (Fig. 7); it can be recycled at least six times without significant decay in original catalytic performance. There is only about a 4% loss of the original catalytic activity for Au/BT catalyst in the 6th reuse, and the transformation efficiency in the 6th reuse remains at a high level with the conversion of 86.4% and TOF of 973 h^{-1}. Compared with the fresh Au/BT, there are almost no changes in phase composition, microstructure, Au particle size, and the chemical state of Au species' surface for the used Au/BT catalyst (Figs. S17–20). These results illustrate Au/BT catalyst's robustness with clean and sustainable solar energy as a sole driving force for the selective photocatalytic hydrogenation of phenylacetylene.

Having demonstrated that Au/BT was an efficient catalyst for selective photocatalytic hydrogenation of phenylacetylene, it was necessary to extend the study to various alkynes with different substituted structures. The results are summarized in Table 2. Reactions of aromatic alkyne involving a methyl group at the 4-position proceeded smoothly to yield the corresponding alkene with the activity of 771 h^{-1} (Table 2, entry 1). Substituent groups in the phenylacetylene framework with steric effect can hinder the transformation under identical conditions [51–63]. 3-hydroxyphenylacetylene and 4-chlorophenylacetylene show moderate performance over Au/BT catalyst (Table 2, entries 2 and 3). These results indicate that the terminal alkynes are relatively active for the downstream conversion. Interestingly, Au/BT's conversion of internal alkynes, such as 1-phenylpropyne, was considerably achieved by Au/BT under the standard reaction reactions (Table 2, entry 4). Besides the aromatic alkynes, the selective photocatalytic hydrogenation of pyridyl substrate was tentatively conducted. As depicted in entry 5, the 2-ethynylpyridine was transformed to the target product with a selectivity of 90.3%. Moreover, the Au/BT can also readily and efficiently convert aliphatic alkyne (e.g., n-decyne) to the corresponding n-decene despite the low catalytic activity of 420 h^{-1} (Table 2, entry 6).

3.3. Structure-activity relationship and reaction mechanism

The correlation between Au–BT interactions and the versatile photocatalyst activity for phenylacetylene semi-hydrogenation was further carried out to gain new insights into the reaction mechanism. Direct KIEs with hydrogen being labeled using D_2 or HD were summarized in Table 3. The HD and D_2 show remarkable KIEs of 1.32 and 2.21, respectively, in the semi-hydrogenation process over Au/BT catalyst. These results indicate that the cleavage of the H−H bond and the activation of the C≡C group, and the formation of C=C and C−C bonds in potential products are kinetically-relevant steps in phenylacetylene hydrogenation [52,59,63–66]. Besides the intrinsic role of Au NPs, the injected hot electrons and strong interactions between Au and BT can also promote the H_2 activation and dissociation and are beneficial for the key hydrogenation steps.

Table 3
KIEs of selective photocatalytic hydrogenation of phenylacetylene using Au/BT.[a].

Entry	Reactants	TOF (h^{-1})	KIE[b]
1	Ph-CCH + H_2	1128	–
2	Ph-CCH + HD	855	1.32
3	Ph-CCH + D_2	509	2.21

[a] Reaction conditions: 40 mg catalyst, 2 mL ethanol, 4.42 mmol phenylacetylene, 2 MPa H_2 or HD or D_2, solar light irradiation at 25 °C for 2 h. The conversions were kept below 20% for the calculation of the initial TOF.
[b] KIE = TOF (Entry 1)/TOF (Entry n) (n = 2 or 3).

To further understand the reaction mechanism and detect the potential key intermediates in the photocatalytic phenylacetylene semi-hydrogenation process over the Au/BT catalyst under solar light irradiation, the in situ diffuse reflectance infrared Fourier transform (DRIFT) spectroscopy was conducted. As shown in Fig. 8a, the two bands occurring at 1040 cm^{-1} of C–H in ≡C–CH group and 1480 cm^{-1} of C–C in phenyl ring are characteristic of the absorption pattern produced by substrate phenylacetylene [67–69]. Three bands at 2825, 2895, and 2954 cm^{-1} are characteristic of C–H bonds of ethylbenzene [67–69]. It should be emphasized that the formation and adsorption of styrene onto the Au/BT surface stimulated by solar light shows a more significant effect than Au/TiO_2 (Fig. 8b) on the positions and relative intensities of the vibrational structure corresponding to the vinyl group. The C=C stretching band at 1645 cm^{-1} and C–H bond at 1595 cm^{-1} as dominated signals both frequency increase with reaction time under light irradiation and approach the equilibrium state in 30 min [68].

Scheme 1 shows the possible reaction steps involved in Au/BT-driven selective photocatalytic phenylacetylene hydrogenation to styrene under solar light irradiation. Initial chemical activation and dissociative adsorption of H_2 molecules, and chemisorption of phenylacetylene on the hot electron injected Au NPs surface primarily through the Au–C (Au/BT–phenylacetylide) interactions, thus significantly facilitating C≡C group activation and leading to the formation of metal–

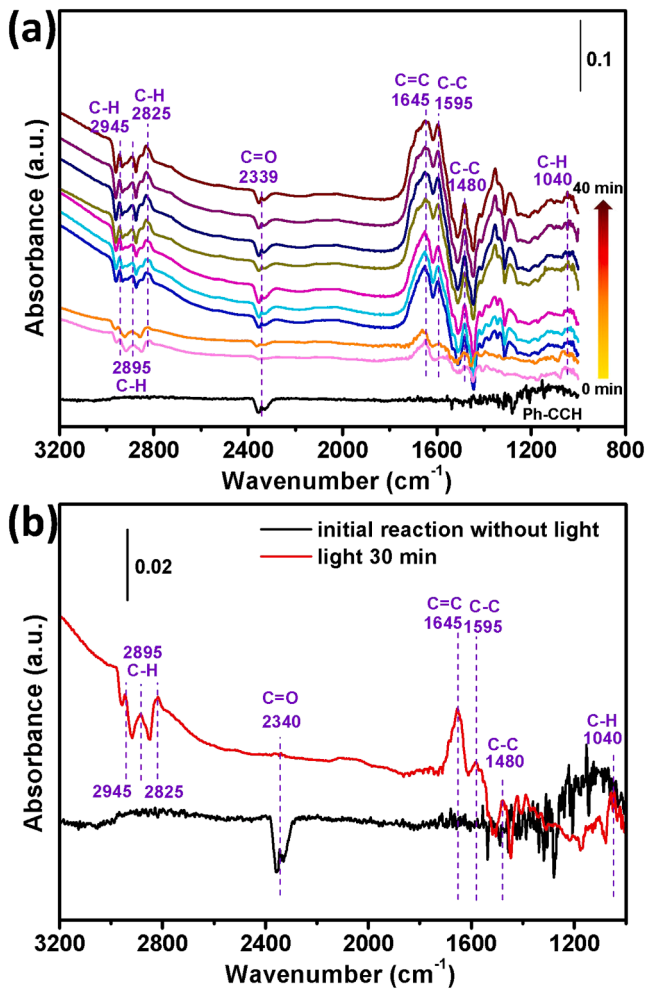

Fig. 8. *In situ* time-resolved DRIFT spectra of photocatalytic phenylacetylene hydrogenation over (a) Au/BT and (b) Au/TiO_2 catalysts.

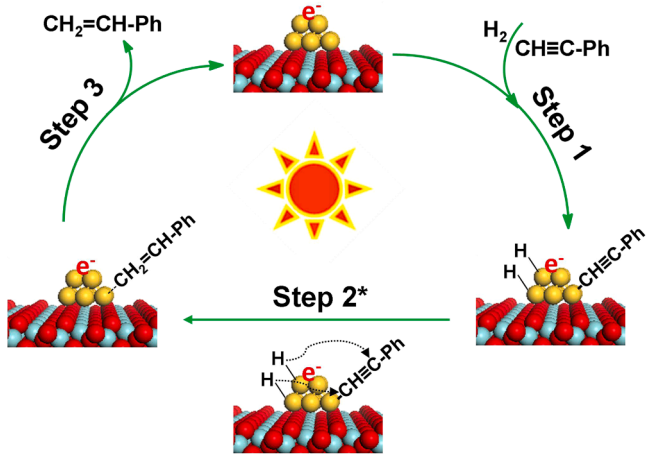

Scheme 1. Possible reaction mechanism for the photocatalytic hydrogenation of phenylacetylene to styrene by using Au/BT catalyst.

phenylacetylide (step 1). The strong Au–BT interactions also favor this abstraction. Phenylacetylide is hydrogenated to generate adsorbed styrene via the hydrogenation of the activated C≡C group (step 2). The hydrogenated product styrene finally desorbs from the Au-based catalyst surface (step 3). The adsorption and chemical activation of H_2 and phenylacetylene molecules are generally considered the kinetically-relevant steps and the C≡C group hydrogenation (step 2) as the rate-determining step (RDS) [52,59,63–66]. Although a considerable amount of energy is necessary for phenylacetylene hydrogenation, the appropriate interaction of Au/BT–phenylacetylide as well as the strong interactions between Au NPs and defective BT substrate could efficiently compromise all the energy barriers, thus achieved the occurrence of target reaction and exhibited the high performance.

4. Conclusions

In summary, we demonstrate that the Au/BT catalyst can efficiently harvest solar energy in selective hydrogenation of alkynes to corresponding unsaturated alkenes with high activity and selectivity. The defective BT material with unique crystalline- core/amorphous-shell (TiO_2@TiO_{2-x}) structure coupled Au NPs shows the broad spectrum response's extraordinary physicochemical properties, considerable carrier concentrations, enhanced separation and transportation of photogenerated e^-–h^+ pairs, and numerous surface oxygen vacancies. The hot electron injection from conductive BT to the surface of plasmonic Au NPs at Au−BT interface stimulated by solar light is critically important. The energetic electrons could powerfully activate the alkynes by contacting the C≡C bonds and directly participating in selective photocatalytic reactions to overcome the energy barriers. The robust Au/BT exhibits outstanding performance for selective hydrogenation of phenylacetylene under solar light irradiation at room temperature, which is much higher than previously reported catalysts. Moreover, Au/BT shows broad scope toward selective photocatalytic hydrogenation of alkyne substrates containing various substituent groups of –CH_3, –OH, –Cl, and so on. Primary KIEs and in situ DRIFTS analysis suggest that the cleavage of H−H bond and the activation of C≡C group and the formation of C=C bond are kinetically-relevant steps, and the latter is the rate-determining step in phenylacetylene conversion. The present work will provide new possibilities for efficient and green alkyne semi-hydrogenation and inspire innovative materials for broader solar-energy-driven chemical transformations.

CRediT authorship contribution statement

Qingyuan Bi: Conceptualization, Investigation, Methodology, Formal analysis, Data curation, Funding acquisition, Writing – original draft. **Erhong Song:** Methodology, Formal analysis, Resources. **Jiacheng Chen:** Formal analysis. **Muhammad Sohail Riaz:** Investigation, Writing – review & editing. **Minghui Zhu:** Methodology, Resources. **Jianjun Liu:** Investigation, Validation. **Yi-Fan Han:** Investigation, Project administration. **Fuqiang Huang:** Conceptualization, Methodology, Funding acquisition, Project administration, Supervision, Writing - review & editing.

Declaration of Competing Interest

The authors declare that they have no known competing financial interests or personal relationships that could have appeared to influence the work reported in this paper.

Acknowledgements

This work was financially supported by the National Natural Science Foundation of China (21872166, 21973107), Shanghai Science and Technology Innovation Action Plan (20dz1204400, 21ZR1472900), and the Key Research Program of the Chinese Academy of Sciences (KGZD-EW-T06 and QYZDJ-SSW-JSC013).

Appendix A. Supporting information

Supplementary data associated with this article can be found in the

online version at doi:10.1016/j.apcatb.2022.121222.

References

[1] F. Studt, F. Abild-Pedersen, T. Bligaard, R.Z. Sørensen, C.H. Christensen, J. K. Nørskov, Identification of non-precious metal alloy catalysts for selective hydrogenation of acetylene, Science 320 (2008) 1320–1322.

[2] C. Oger, L. Balas, T. Durand, J.M. Galano, Are alkyne reductions chemo-, regio-, and stereoselective enough to provide pure (*Z*)-olefins in polyfunctionalized bioactive molecules? Chem. Rev. 113 (2013) 1313–1350.

[3] M. Jorgensen, H. Gronbeck, Selective acetylene hydrogenation over single-atom alloy nanoparticles by kinetic monte carlo, J. Am. Chem. Soc. 141 (2019) 8541–8549.

[4] K. Su, Y. Wang, C. Zhang, Z. Gao, J. Han, F. Wang, Tuning the Pt species on Nb_2O_5 by support-induced modification in the photocatalytic transfer hydrogenation of phenylacetylene, Appl. Catal. B: Environ. 298 (2021), 120554.

[5] M. Crespo-Quesada, F. Cárdenas-Lizana, A.L. Dessimoz, L. Kiwi-Minsker, Modern trends in catalyst and process design for alkyne hydrogenations, ACS Catal. 2 (2012) 1773–1786.

[6] G. Vilé, D. Albani, N. Almora-Barrios, N. López, J. Pérez-Ramírez, Advances in the design of nanostructured catalysts for selective hydrogenation, ChemCatChem 8 (2016) 21–33.

[7] M. Hu, Z. Wu, Z. Yao, J. Young, L. Luo, Y. Du, C. Wang, Z. Iqbal, X. Wang, N_8 stabilized single-atom Pd for highly selective hydrogenation of acetylene, J. Catal. 395 (2021) 46–53.

[8] L. Jiang, K. Liu, S.F. Hung, L. Zhou, R. Qin, Q. Zhang, P. Liu, L. Gu, H.M. Chen, G. Fu, N. Zheng, Facet engineering accelerates spillover hydrogenation on highly diluted metal nanocatalysts, Nat. Nanotechnol. 15 (2020) 848–853.

[9] R. Lin, D. Albani, E. Fako, S.K. Kaiser, O.V. Safonova, N. López, J. Pérez-Ramírez, Design of single gold atoms on nitrogen-doped carbon for molecular recognition in alkyne semi-hydrogenation, Angew. Chem. Int. Ed. 58 (2019) 504–509.

[10] L. Zhang, M. Zhou, A. Wang, T. Zhang, Selective hydrogenation over supported metal catalysts: from nanoparticles to single atoms, Chem. Rev. 120 (2020) 683–733.

[11] M. Li, N. Zhang, R. Long, W. Ye, C. Wang, Y. Xiong, PdPt alloy nanocatalysts supported on TiO_2 maneuvering metal–hydrogen interactions for light-driven and water-donating selective alkyne semihydrogenation, Small 13 (2017), 1604173.

[12] Z. Wang, H. Wang, Y. Shi, C. Liu, L. Wu, CuPd alloy decorated $SnNb_2O_6$ nanosheets as a multifunctional photocatalyst for semihydrogenation of phenylacetylene under visible light, Chem. Eng. J. 429 (2022), 132018.

[13] L. Liu, X. Chen, Titanium dioxide nanomaterials: self-structural modifications, Chem. Rev. 114 (2014) 9890–9918.

[14] Y. Ma, X. Wang, Y. Jia, X. Chen, H. Han, C. Li, Titanium dioxide-based nanomaterials for photocatalytic fuel generations, Chem. Rev. 114 (2014) 9987–10043.

[15] J. Wang, Y. Li, L. Deng, N. Wei, Y. Weng, S. Dong, D. Qi, J. Qiu, X. Chen, T. Wu, High-performance photothermal conversion of narrow-bandgap Ti_2O_3 nanoparticles, Adv. Mater. 29 (2017), 1603730.

[16] S. Selcuk, X. Zhao, A. Selloni, Structural evolution of titanium dioxide during reduction in high-pressure hydrogen, Nat. Mater. 17 (2018) 923–928.

[17] K. Lan, R. Wang, Q. Wei, Y. Wang, A. Hong, P. Feng, D. Zhao, Stable Ti^{3+} defects in oriented mesoporous titania frameworks for efficient photocatalysis, Angew. Chem. Int. Ed. 59 (2020) 17676–17683.

[18] X. Chen, L. Liu, P.Y. Yu, S.S. Mao, Increasing solar absorption for photocatalysis with black hydrogenated titanium dioxide nanocrystals, Science 331 (2011) 746–750.

[19] G. Liu, L.C. Yin, J. Wang, P. Niu, C. Zhen, Y. Xie, H.M. Cheng, A red anatase TiO_2 photocatalyst for solar energy conversion, Energy Environ. Sci. 5 (2012) 9603–9610.

[20] G. Jia, Y. Wang, X. Cui, H. Zhang, J. Zhao, L.H. Li, L. Gu, Q. Zhang, L. Zheng, J. Wu, Q. Wu, D.J. Singh, W. Li, L. Zhang, W. Zheng, Wet-chemistry hydrogen doped TiO_2 with switchable defects control for photocatalytic hydrogen evolution, Matter 5 (2022) 206–218.

[21] S.K. Cushing, F. Meng, J. Zhang, B. Ding, C.K. Chen, C.J. Chen, R.S. Liu, A. D. Bristow, J. Bright, P. Zheng, N. Wu, Effects of defects on photocatalytic activity of hydrogen-treated titanium oxide nanobelts, ACS Catal. 7 (2017) 1742–1748.

[22] T.D. Nguyen, J. Li, E. Lizundia, M. Niederberger, W.Y. Hamad, M.J. MacLachlan, Black titania with nanoscale helicity, Adv. Funct. Mater. 29 (2019), 1904639.

[23] X. Chen, L. Liu, F. Huang, Black titanium dioxide (TiO_2) nanomaterials, Chem. Soc. Rev. 44 (2015) 1861–1885.

[24] X. Liu, G. Zhu, X. Wang, X. Yuan, T. Lin, F. Huang, Progress in black titania: a new material for advanced photocatalysis, Adv. Energy Mater. 6 (2016), 1600452.

[25] Z. Wang, C. Yang, T. Lin, H. Yin, P. Chen, D. Wan, F. Xu, F. Huang, J. Lin, X. Xie, M. Jiang, H-doped black titania with very high solar absorption and excellent photocatalysis enhanced by localized surface plasmon resonance, Adv. Funct. Mater. 23 (2013) 5444–5450.

[26] C. Yang, Z. Wang, T. Lin, H. Yin, X. Lü, D. Wan, T. Xu, C. Zheng, J. Lin, F. Huang, X. Xie, M. Jiang, Core-shell nanostructured "black" rutile titania as excellent catalyst for hydrogen production enhanced by sulfur doping, J. Am. Chem. Soc. 135 (2013) 17831–17838.

[27] G. Yin, Q. Bi, W. Zhao, J. Xu, T. Lin, F. Huang, Efficient conversion of CO_2 to methane photocatalyzed by conductive black titania, ChemCatChem 9 (2017) 4389–4396.

[28] G. Yin, X. Huang, T. Chen, W. Zhao, Q. Bi, J. Xu, Y. Han, F. Huang, Hydrogenated blue titania for efficient solar to chemical conversions: preparation, characterization, and reaction mechanism of CO_2 reduction, ACS Catal. 8 (2018) 1009–1017.

[29] Q. Bi, K. Hu, J. Chen, Y. Zhang, M.S. Riaz, J. Xu, Y. Han, F. Huang, Black phosphorus coupled black titania nanocomposites with enhanced sunlight absorption properties for efficient photocatalytic CO_2 reduction, Appl. Catal. B: Environ. 295 (2021), 120211.

[30] Z. Ma, S. Dai, Heterogeneous Gold Catalysts And Catalysis, The Royal Society of Chemistry, Cambridge, 2014.

[31] Y. Wei, M. Shi, Divergent synthesis of carbo- and heterocycles via gold- catalyzed reactions, ACS Catal. 6 (2016) 2515–2524.

[32] M. Sankar, Q. He, R.V. Engel, M.A. Sainna, A.J. Logsdail, A. Roldan, D.J. Willock, N. Agarwal, C.J. Kiely, G.J. Hutchings, Role of the support in gold-containing nanoparticles as heterogeneous catalysts, Chem. Rev. 120 (2020) 3890–3983.

[33] S. Witzel, A.S.K. Hashmi, J. Xie, Light in gold catalysis, Chem. Rev. 121 (2021) 8868–8925.

[34] P. Christopher, H. Xin, S. Linic, Visible-light-enhanced catalytic oxidation reactions on plasmonic silver nanostructures, Nat. Chem. 3 (2011) 467–472.

[35] C.H. Hao, X.N. Guo, Y.T. Pan, S. Chen, Z.F. Jiao, H. Yang, X.Y. Guo, Visible- light-driven selective photocatalytic hydrogenation of cinnamaldehyde over Au/SiC catalysts, J. Am. Chem. Soc. 138 (2016) 9361–9364.

[36] J. Yang, Y. Guo, R. Jiang, F. Qin, H. Zhang, W. Lu, J. Wang, J.C. Yu, High-efficiency "working-in-tandem" nitrogen photofixation achieved by assembling plasmonic gold nanocrystals on ultrathin titania nanosheets, J. Am. Chem. Soc. 140 (2018) 8497–8508.

[37] M. Gong, M. Alamri, D. Ewing, S.M. Sadeghi, J.Z. Wu, Localized surface plasmon resonance enhanced light absorption in AuCu/$CsPbCl_3$ core/shell nanocrystals, Adv. Mater. 32 (2020), 2002163.

[38] Y. Zhang, S. He, W. Guo, Y. Hu, J. Huang, J.R. Mulcahy, W.D. Wei, Surface-plasmon-driven hot electron photochemistry, Chem. Rev. 118 (2018) 2927–2954.

[39] L. Zhou, D.F. Swearer, C. Zhang, H. Robatjazi, H. Zhao, L. Henderson, L. Dong, P. Christopher, E.A. Carter, P. Nordlander, N.J. Halas, Quantifying hot carrier and thermal contributions in plasmonic photocatalysis, Science 362 (2018) 69–72.

[40] C. Zhan, Q.X. Wang, J. Yi, L. Chen, D.Y. Wu, Y. Wang, Z.X. Xie, M. Moskovits, Z. Q. Tian, Plasmonic nanoreactors regulating selective oxidation by energetic electrons and nanoconfined thermal fields, Sci. Adv. 7 (2021) eabf0962.

[41] J. Wang, L. Wang, S. Yu, T. Ding, D. Xiang, K. Wu, Spin blockade and phonon bottleneck for hot electron relaxation observed in *n*-doped colloidal quantum dots, Nat. Commun. 12 (2021) 550.

[42] Q.Y. Bi, X.L. Du, Y.M. Liu, Y. Cao, H.Y. He, K.N. Fan, Efficient subnanometric gold-catalyzed hydrogen generation via formic acid decomposition under ambient conditions, J. Am. Chem. Soc. 134 (2012) 8926–8933.

[43] G. Kresse, J. Furthmüller, Efficient iterative schemes for ab initio total-energy calculations using a plane-wave basis set, Phys. Rev. B 54 (1996) 11169.

[44] P.E. Blöchl, Projector augmented-wave method, Phys. Rev. B 50 (1994) 17953.

[45] A. Naldoni, M. Allieta, S. Santangelo, M. Marelli, F. Fabbri, S. Cappelli, C. L. Bianchi, R. Psaro, V.D. Santo, Effect of nature and location of defects on bandgap narrowing in black TiO_2 nanoparticles, J. Am. Chem. Soc. 134 (2012) 7600–7603.

[46] J. Chen, M. Gong, Y. Fan, J. Feng, L. Han, H.L. Xin, M. Cao, Q. Zhang, D. Zhang, D. Lei, Y. Yin, Collective plasmon coupling in gold nanoparticle clusters for highly efficient photothermal therapy, ACS Nano 16 (2022) 910–920.

[47] W. Liang, W. Qin, D. Li, Y. Wang, W. Guo, Y. Bi, Y. Sun, L. Jiang, Localized surface plasmon resonance enhanced electrochemical nitrogen reduction reaction, Appl. Catal. B: Environ. 301 (2022), 120808.

[48] Z. Jin, Q. Wang, W. Zheng, X. Cui, Highly ordered periodic Au/TiO_2 hetero-nanostructures for plasmon-induced enhancement of the activity and stability for ethanol electro-oxidation, ACS Appl. Mater. Interfaces 8 (2016) 5273–5279.

[49] S. Mukherjee, L. Zhou, A.M. Goodman, N. Large, C. Ayala-Orozco, Y. Zhang, P. Nordlander, N.J. Halas, Hot-electron-induced dissociation of H_2 on gold nanoparticles supported on SiO_2, J. Am. Chem. Soc. 136 (2014) 64–67.

[50] Q. Bi, J. Lin, Y. Liu, H. He, F. Huang, Y. Cao, Dehydrogenation of formic acid at room temperature: boosting palladium nanoparticle efficiency by coupling with pyridinic-nitrogen-doped carbon, Angew. Chem. Int. Ed. 55 (2016) 11849–11853.

[51] D. Albani, M. Shahrokhi, Z. Chen, S. Mitchell, R. Hauert, N. López, J. Pérez-Ramírez, Selective ensembles in supported palladium sulfide nanoparticles for alkyne semi-hydrogenation, Nat. Commun. 9 (2018) 2634.

[52] X. Zhao, L. Zhou, W. Zhang, C. Hu, L. Dai, L. Ren, B. Wu, G. Fu, N. Zheng, Thiol treatment creates selective palladium catalysts for semihydrogenation of internal alkynes, Chem 4 (2018) 1080–1091.

[53] C. Riley, S. Zhou, D. Kunwar, A.D.L. Riva, E. Peterson, R. Payne, L. Gao, S. Lin, H. Guo, A. Datye, Design of effective catalysts for selective alkyne hydrogenation by doping of ceria with a single-atom promotor, J. Am. Chem. Soc. 140 (2018) 12964–12973.

[54] F. Huang, Y. Deng, Y. Chen, X. Cai, M. Peng, Z. Jia, P. Ren, D. Xiao, X. Wen, N. Wang, H. Liu, D. Ma, Atomically dispersed Pd on nanodiamond/graphene hybrid for selective hydrogenation of acetylene, J. Am. Chem. Soc. 140 (2018) 13142–13146.

[55] M. Yan, T. Jin, Y. Ishikawa, T. Minato, T. Fujita, L.Y. Chen, M. Bao, N. Asao, M. W. Chen, Y. Yamamoto, Nanoporous gold catalyst for highly selective semihydrogenation of alkynes: remarkable effect of amine additives, J. Am. Chem. Soc. 134 (2012) 17536–17542.

[56] P.V. Markov, I.S. Mashkovsky, G.O. Bragina, J. Wärnå, E.Yu Gerasimov, V. I. Bukhtiyarov, A.Yu Stakheev, D.Yu Murzin, Particle size effect in liquid-phase hydrogenation of phenylacetylene over Pd catalysts: experimental data and theoretical analysis, Chem. Eng. J. 358 (2019) 520–530.

[57] B. Li, H. Ge, Highly selective electrochemical hydrogenation of alkynes: rapid construction of mechanochromic materials, Sci. Adv. 5 (2019) eaaw2774.

[58] X.K. Wan, J.Q. Wang, Z.A. Nan, Q.M. Wang, Ligand effects in catalysis by atomically precise gold nanoclusters, Sci. Adv. 3 (2017), e1701823.
[59] S. Wei, A. Li, J.C. Liu, Z. Li, W. Chen, Y. Gong, Q. Zhang, W.C. Cheong, Y. Wang, L. Zheng, H. Xiao, C. Chen, D. Wang, Q. Peng, L. Gu, X. Han, J. Li, Y. Li, Direct observation of noble metal nanoparticles transforming to thermally stable single atoms, Nat. Nanotechnol. 13 (2018) 856–861.
[60] B. Zhang, H. Asakura, J. Zhang, J. Zhang, S. De, N. Yan, Stabilizing a platinum$_1$ single-atom catalyst on supported phosphomolybdic acid without compromising hydrogenation activity, Angew. Chem. Int. Ed. 55 (2016) 8319–8323.
[61] S. Ji, Y. Chen, S. Zhao, W. Chen, L. Shi, Y. Wang, J. Dong, Z. Li, F. Li, C. Chen, Q. Peng, J. Li, D. Wang, Y. Li, Atomically dispersed ruthenium species inside metal–organic frameworks: combining the high activity of atomic sites and the molecular sieving effect of MOFs, Angew. Chem. Int. Ed. 58 (2019) 4271–4275.
[62] S. Wang, Z.J. Zhao, X. Chang, J. Zhao, H. Tian, C. Yang, M. Li, Q. Fu, R. Mu, J. Gong, Activation and spillover of hydrogen on sub-1nm palladium nanoclusters confined within sodalite zeolite for the semi-hydrogenation of alkynes, Angew. Chem. Int. Ed. 58 (2019) 7668–7672.
[63] K. Choe, F. Zheng, H. Wang, Y. Yuan, W. Zhao, G. Xue, X. Qiu, M. Ri, X. Shi, Y. Wang, G. Li, Z. Tang, Fast and selective semihydrogenation of alkynes by palladium nanoparticles sandwiched in metal–organic frameworks, Angew. Chem. Int. Ed. 59 (2020) 3650–3657.
[64] K. Werner, X. Weng, F. Calaza, M. Sterrer, T. Kropp, J. Paier, J. Sauer, M. Wilde, K. Fukutani, S. Shaikhutdinov, H.J. Freund, Toward an understanding of selective alkyne hydrogenation on ceria: on the impact of O vacancies on H_2 interaction with CeO_2(111), J. Am. Chem. Soc. 139 (2017) 17608–17616.
[65] J.L. Fiorio, R.V. Gonçalves, E. Teixeira-Neto, M.A. Ortuño, N. López, L.M. Rossi, Accessing frustrated Lewis pair chemistry through robust gold@N-doped carbon for selective hydrogenation of alkynes, ACS Catal. 8 (2018) 3516–3524.
[66] C.S. Wondergem, T. Hartman, B.M. Weckhuysen, *In situ* shell-isolated nanoparticle-enhanced Raman spectroscopy to unravel sequential hydrogenation of phenylacetylene over platinum nanoparticles, ACS Catal. 9 (2019) 10794–10802.
[67] W.P. Addiego, C.A. Estrada, D.W. Goodman, M.P. Rosynek, R.G. Windham, An infrared study of the dehydrogenation of ethylbenzene to styrene over iron-based catalysts, J. Catal. 146 (1994) 407–414.
[68] R. Jordan, A. Ulman, J.F. Kang, M.H. Rafailovich, J. Sokolov, Surface-initiated anionic polymerization of styrene by means of self-assembled monolayers, J. Am. Chem. Soc. 121 (1999) 1016–1022.
[69] W. Liu, C.O. Arean, S. Bordiga, E. Groppo, A. Zecchina, Selective phenylacetylene hydrogenation on a polymer-supported palladium catalyst monitored by FTIR spectroscopy, ChemCatChem 3 (2011) 222–226.